STUDIA GEOMORPHOLOGICA CARPATHO-BALCANICA
Vol. LI/LII, 2017/2018: 87–105 PL ISSN 0081-6434

ISTVAN P. KOVÁCS[1*], TITUSZ BUGYA[1], SZABOLCS CZIGÁNY[2], MARCO DEFILIPPI[3], BERNADETT DOBRE[1], SZABOLCS ÁKOS FÁBIÁN[2], DENES LÓCZY[2], PAOLO RICCARDI[3], LEVENTE RONCZYK[1], PAOLO PASQUALI[3] (HUNGARY, SWITZERLAND)

MONITORING LANDSLIDES USING C-BAND INTERFEROMETRY. A CASE STUDY: DUNASZEKCSŐ LANDSLIDE, SOUTHERN TRANSDANUBIA, HUNGARY

Abstract. As a tool for high precision deformation monitoring in broader areas, interferometric (InSAR) time series of space-born Synthetic aperture radar (SAR) imagery are used. Nowadays, ERS, Envisat archives and Sentinel-1 images are open for the public to analyse slow moving landslides activated between 1990 and 2017. Since Sentinel-1 satellites are considered to be the workhorse of EO by the ESA during next decades, it is important to assess its applicability in landslide monitoring and mapping. In this paper, the southern part of Dunaszekcső village was analysed with PSI interferometric stacking algorithm, using SAR imagery. The advantages and limitations of the applied interferometric stacking techniques and sensors have been analysed, such as the movement history of the test site between 1992 and 2017. It was proven that Sentinel-1 PSI scatterers far exceeds the spatial coverage obtained by earlier sensors. Two orbital geometries of Sentinel-1 enabled larger spatial coverage and extract 2D displacements. The comparison of the two geometries, however, was only possible for small surfaces in the area of interest. The displacement data in the central part of the study site indicate the subsidence of the sliding block along the escarpment and in the east its movement towards the Danube. This displacement then triggered the uplift of the floodplain edges, or generated a slight eastward displacement.

Keywords: ERS, Envisat, Sentinel-1, PSI, landslide, high bluff

INTRODUCTION AND OBJECTIVES

Remotely sensed data (othophotographs, LiDAR imagery and GPS measurements) are highly instrumental in mapping and monitoring landslides (Glade et al. 2005). However, non-optical satellites, employing radar signals, have been more frequently used in surface deformation studies. Since the launch of SEASAT satellite equipped with Synthetic Aperture Radars (SAR) in 1978, such analytical approaches became widespread. The ERS satellite mission began in the early 1990s, then Envisat satellites were put into operation in the 2000s. These satellites were the pioneers of high resolution observation and monitoring of land deformations and the development of interferometric systems. With the

visualization of the imagery taken at C-band slow, extremely slow and extensive landslides also become detectable (Wasowski, Bowenga 2015).

Conventional analytical techniques, like interferometry (InSAR) or differential interferometry (DInSAR) use the coherence based on satellite image pairs to monitor motions. Coherence and phase difference are also the major attributes of other advanced analytical techniques. Nonetheless, the efficiency of InSAR and DInSAR systems is limited by several factors. Spatial and temporal coherence and motion data are regularly mitigated or corrupted by temporal decorrelation, atmospheric noise and topography (Hein 2004). With advanced interferometric stacking methods, a series of SAR images are analysed at the same time, enabling the elimination of the majority of the above-mentioned issues (atmospheric noise and the effect of topography). A widely used algorithm of this type is persistent scatterers (PS), introduced by A. Feretti et al. (2001), which has become one of the standard procedures in landslide mapping and monitoring.

The Copernicus Program of the European Space Agency, and the Sentinel satellite family launched within that framework, opened a new era in Earth observation. Sentinel 1-A satellites take images of the Earth surface at a 12 day interval. It was shortened to 6 days by the Sentinel 1-B mission. New advanced sensor and imagery techniques as well as the novel, modified orbital geometry (low base line and orbital tube) provides many challenges for the analysers. Therefore, we have limited information available on the accuracy of the interferometric methods (Herrera et al. 2010; Herrera et al. 2013; Chen et al. 2014; Singleton et al. 2014; Tomás et al. 2014; Sowter et al. 2016;) and their role in landslide mapping and monitoring.

During the Middle Pleistocene, the main flow direction of the Danube turned to south and induced active erosion along the edge of the Mezőföld and the South Baranya Hills (Pécsi 1959). As a consequence, a series of 20 to 60-meter-high bluffs were formed along the right bank of the Danube. The total length of the high bluffs reaches 86 km (Kenesei et al. 2005). The high bluffs are composed of Late Miocene (Pannonian) lacustrine (clayey and silty) sediments, Pliocene red and reddish clays and Pleistocene loess and paleosol series (Pécsi 1956, 1959). The extremely high phyllosilicate (illite, montmorillonite and kaolinite) content of the sediments, the water saturation and undercutting due to the proximity of the Danube create ideal circumstances for the generation of landslides. These processes intensely shape the high bluffs along the right bank of the Danube (Karácsonyi, Scheuer 1972). To date, geomorphologic research has focused on the active development of the high bluff section between the villages of Kulcs and Rácalmás and especially at the village of Dunaszekcső (Újvári et al. 2009; Balogh, Schweitzer 2011). In the 1970s and 1980s researchers were primarily concerned with the general description of the mass movements (Schmiedt 1966; Egri, Párdányi 1968; Tóthné-Scheuer, Vermes 1968; Kézdi 1970; Pécsi 1971; Horváth, Scheuer 1976; Fodorné et al. 1981). Several papers strived to trace the triggering factors behind these geomorphic

processes (Karácsonyi, Scheuer 1972; Györké et al. 1975; Horváth et al. 1975; Horváth, Scheuer 1976; Scheuer 1979; Fodorné et al. 1981). Only sporadic information is available on the geomorphic evolution of the high bluffs today, since monitoring stations for the temporal tracking movements were only established in the town of Dunaújváros and the village of Dunaszekcső (Újvári et al. 2009; Bugya et al. 2011; Bányai et al 2014; Kovács et al. 2015). Monitoring, however, has only covered relatively small surfaces and is generally based on field survey methods (geodetic data acquisition and DGSP measurements). Nonetheless, scientific analyses of remotely sensed data, with the exception of the work of C. Del Ventisette et al. (2013) on the Rácalmás high bluffs, have not yet been carried out in Hungary. Although major efforts and financial resources have already been invested by local governments into the stabilization of the actively moving sections of high bluffs, due to the limited availability of scientific data and the low coherence of the high bluffs, the prediction of the rates and locations of future movements remains unsolved.

The objective of the current exploratory study was to adopt freely-available C-band SAR images for the mapping and monitoring of the stability of the landslide-prone high bluffs at Dunaszekcső. We also aimed at exploring the spatial and temporal behaviour of the detected deformations.

SITE DESCRIPTION

The southernmost member of the Hungarian high bluff series along the Hungarian reach of the Danube is the Mohács-Báta high bluff series, formed between the depressions of Sárköz and Mohács, and stretches for a length of about 15 km (Moyzes, Scheuer 1978; Dövényi 2010). The village of Dunaszekcső is situated in the central part of the high bluff series. The most elevated part of the high bluffs, the Vár Hill, is situated in the northern part of the village at an altitude of about 140 meters a.m.s.l, about 60 meters above the mean water level of the Danube (Fig. 1). To the north and the west of the high bluffs the Lánka Stream flows into the Danube. No river terrace has been formed anywhere between the Danube and the high bluffs along the Dunaszekcső study site. Therefore, here the evolution of the high bluffs is directly influenced by the Danube.

South of the confluence of the Lánka Stream, the loess plateau is lowered, and only elevated by 15 to 20 meters above its surroundings to an altitude of about 120 meters a.m.s.l.

The river bank in Dunaszekcső is built up of the series of Pleistocene loess and paleosols of 100 m thickness, superpositioned on the underlying Pliocene red clays and Pannonian clayey sediments positioned below the mean level of the Danube at 82 m a.m.s.l. (Pécsi, Schweitzer 1995). The Dunaszekcső site is the only member of the Hungarian high bluff series where landslides took place on Pleistocene sediments (Moyzes, Scheuer 1978). The residential

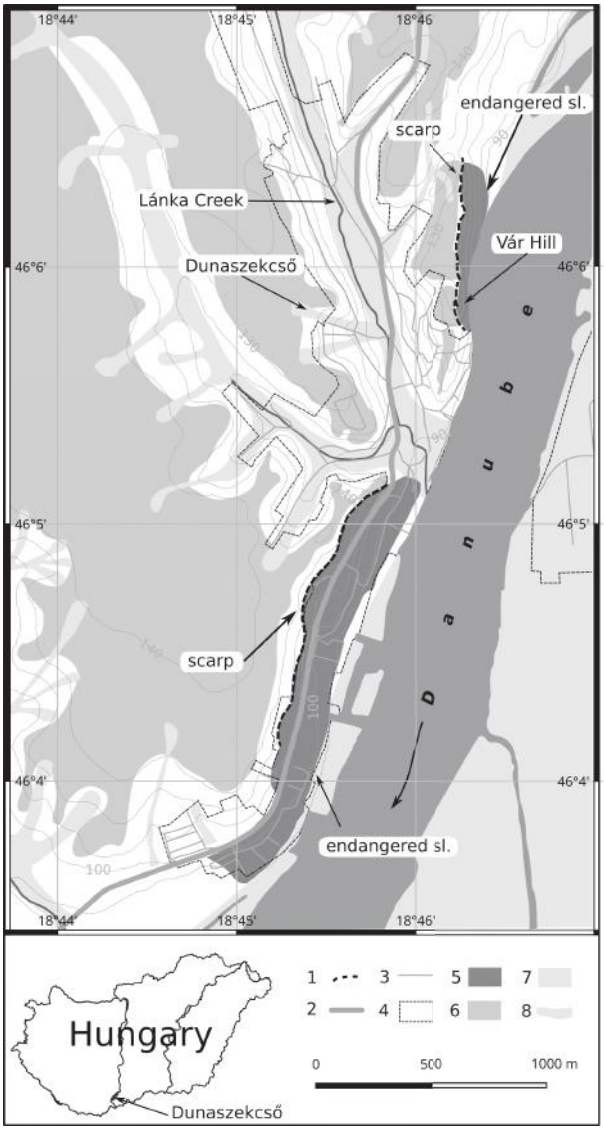

Fig. 1: Location map of Dunaszekcső. 1= main bluff, 2 = primarily road, 3 = secondary, tertiary and residential roads, 4 = residential area, 5 = endangered slope with recent landslides, 6 = loess plateau, 7 = floodplain, island, 8 = valley

areas of Dunaszekcső are located in the valley of the Lánka Stream, the adjacent sloping surfaces and the stable western slopes of the Vár Hill, as well as in front of the high bluffs on the landslide blocks to the south. Land use in the broader vicinity of the village is dominated by farmlands and floodplain forests.

According to F. Kaszás and J. Kraft (2009) and J. Kraft (2011) the first documented landslides in Dunaszekcső date back to the period of the second

military survey (1860s). Later, large and well-documented mass movements were recognized on multiple occasions in 1965, 1976, 2008 and 2011, however all movements were associated with the sediments of the Vár Hill. Landslides on the Vár Hill have occurred repeatedly since their most recent initiation in 2006. A nearly $0.5 \cdot 10^6$ m^3 block of the Vár Hill slid almost 9 meters within few hours in 2008 (Újvári et al. 2009). Additional ruptures appeared in 2011 in the formerly stable surface behind the current block escarpment face (Kovács et al. 2015). The southern part of the currently active block of 30 m width and 100 m long has moved 4 meters vertically between 2011 and 2016. The majority of the movement occurred in 2016 at a mean rate of 0.5 mm per day (authors' unpublished data).

South of the actively moving zone, the older bank section was partly structurally stabilized and terraced at a costs of approximately 300 million HUF (about 1 million Euros), the removed sediments were deposited in the bottom of the escarpment and the slopes of the currently active block. Nevertheless, hitherto only the Vár Hill section of the high bluffs were analysed in details, no data on movement rates are available for the broader vicinity of the Vár Hill. Therefore, the current study aims to analyse the area south of the Vár Hill landslide. The landslide-affected surface covers an area of 0.358 km^2 which equals to about 22% of the entire land surface of the village (1.559 km^2).

Despite the abundance of monitored data on the Vár Hill, our research does not study the mass movement processes of the hill. Although interferometric data could easily be verified by ground measurements, still, waves are scattered and diverted by the dynamic changes of vegetation and only a small fraction returns to the satellite, consequently loss of coherence occurs, which makes data unsuitable for further processing and analysis. Furthermore, with adequate land cover (e.g. corner reflectors placed on the landslide blocks) a sufficient level of coherence is maintained, while at the same time, based on our field survey, the rate of mass movements exceeds the wavelength-determined detection limits of the sensors.

MATERIALS AND METHODS

SATELLITE IMAGES

The available C-band ERS-1, ERS-2, Envisat-1 and Envisat-2 images were downloaded via the Eolisa client. The 41 ERS images, taken on descending orbits covers the period of 1992 to 1999, while 28 Envisat images of ascending orbits were taken between 2002 and 2010.

The mean temporal baseline (Bt) of the ERS images is around 70 days, while for the ascending Envisat images it was increased to 105 days (Table 1).

The Sentinel-1 mission was launched in October, 2014 therefore the minimum number of 20 images that enables the successful operation of the PS procedure, were already available in 2015. Twenty images, however, cover only a short

Table 1

Temporal distribution of the analysed images at Dunaszekcső (based on own sources).

		ERS-1/2 descending	Envisat-1/2 ascending	Envisat-1/2 descending	Sentinel-1A ascending	Sentinel-1A descending
Time of imaging	**First image**	1992.06.18	2002.11.17	2002.11.01	2014.10.29	2014.10.21
	Last image	1999.11.28	2010.09.26	2010.09.10	2017.08.26	2016.08.24
Number of images		41	28	41	106	98
Time lapse between image acquisitions	**Minimum**	1	35	35	6	6
	Maximum	548	525	350	36	48
	Standard Deviation	92	98	66	5	7
	Mean	68	106	72	10	11
	Median	35	70	35	6	6

period of time, insufficient for the filtering of the aforementioned atmospheric noise. An additional problem is that many pictures were taken during the active vegetative phase, due to which significant coherence loss is expected. To mitigate the effect of the previously mentioned noises, in the current study we analysed all available time series data covering the entire 3-year period.

The Sentinel-1A single look complexes (SLC) acquired in Interferometric Wide (IW) swath were downloaded from ESA's Sentinels Scientific Data Hub (https://scihub.copernicus.eu). Terrain Observation with Progressive Scan SAR (TOPSAR) processing method was used for Sentinel-1 images. This method is different from the once widely employed ScanSAR (ERS, Envisat) algorithm. In this imaging method each satellite-acquired image is composed of multiple bursts (ESA 2013). Each burst overlaps with its bordering neighbours. Therefore, the overlap provides sufficient coverage for the entire image. During the processing instead of the entire image only the necessary bursts were imported; therefore, calculation capacity and time were significantly reduced.

The Sentinel SLCs span a period of three years (Fig. 2). Average return times of the satellites in Dunaszekcső site ranged between 10 to 11 days (12-day for Sentinel-1, later, when Sentinel-2 was launched, it was reduced to 6 days). This provides a unique opportunity for the detection of surface movements where movement rates are less than 2.8 cm per 10–11 days.

It should be noted that ERS and Envisat imagery offers a spatial resolution of 25 m, while Sentinel-1 sensors provide a more enhanced 15 m raw resolution for interferometric processing.

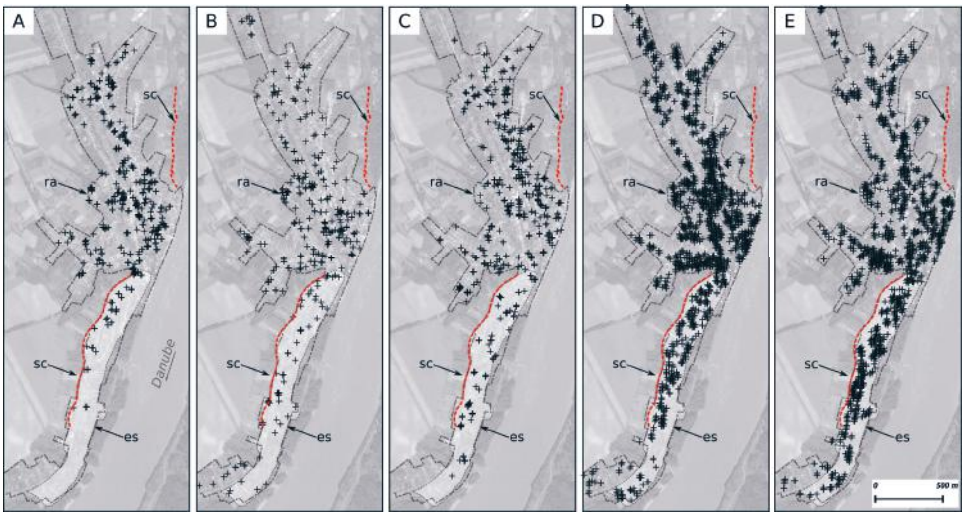

Fig. 2. Spatial distribution of detected scatterers after data processing. A = ERS descending geometry, B= Envisat ascending geometry, C = Envisat descending geometry, D = Sentinel-1 ascending geometry, E = Sentinel-1 descending geometry, ra = residential area, sc = scarp, es = landslide-affected slope

METHODOLOGY

During the current study surface deformations observed in the village of Dunaszekcső were analysed with the SARscape 5.4.0. add-in module of the Envi 5.4.1 software. The persistent scatterer (PSI) procedure, built in the module, was carried out on the ERS, Envisat and Sentinel-1 images. The phase signals, acquired by SAR antennas and used for the detection of ground surface deformations, are determined by the following parameters:

$$\Delta\varphi_{i}(x,y) = \Delta\varphi_{disp} + \Delta\varphi_{topo} + \Delta\varphi_{atm} + \varphi_{res};$$

where $\Delta\varphi$ is the phase, $\Delta\varphi_{disp}$ = is ground displacement, $\Delta\varphi_{topo}$ = topography, $\Delta\varphi_{atm}$ = atmospheric noise, φ_{res} = residual noise.

Topography and atmospheric noise significantly influences the detection of displacements. It is a major issue for the conventional InSAR and DInSAR procedures, where only a limited possibility exists for their filtering. Therefore, the PSI algorithm uses multiple image pairs (interferograms) for the quantification and the filtering of the atmospheric noise and impact of topography.

Although our research site only covers an area of a few km^2, a larger area of about 15×20 km was used for the analyses of the satellite images. The reason for the use of the extended area was to enable the successful land dissection at grid sizes of 5×5 km in the second stage of the processing algorithm, and to achieve satisfactory efficiency during filtering (convolution matrixes).

To remove the topography phase and unpack the interferograms, the SRTM-v4 digital terrain model was used. Nevertheless, the resolution and quality

of the terrain model fundamentally determines the success rate of the removal of the topographic phase and the accuracy of the final displacement data.

The PSI algorithm used in SARScape is based on the permanent scatterer technique, developed by Ferreti et al (2001). This algorithm in general seeks point-like reflective areas of distinct geometry, where coherence permanently maintained over the period of interest (Pasquali et al. 2014). Such objects typically include houses and other engineering structures in residential areas. Nonetheless, for the successful removal of atmospheric noise displacements need to be modelled which is only feasible in a linear fashion for the PSI. The non-modelled components are likely removed by the atmospheric filter (Ferreti. 2014). Therefore, the PSI method only provides true results for linear surface displacements. In general, atmospheric noise is well correlated in space but poorly in time. Hence, it can be filtered with both spatial and temporal convolution matrixes (Ferreti et al. 2000). However, by increasing the efficiency of noise filtering significant data loss may occur, therefore, filter setting was prepared with extreme caution (365 days and 1,200 m).

For the geocoding of Sentinel-1A data a coherence of 0.75 and pixel size of 15 m were used, while for earlier sensors coherence of 0.62 and pixel size of 25 meter were found the most satisfactory.

Our results are presented in the form of a 1-dimensional line of loss (LOS) velocities, which, with the adequate sign (negative or positive) describe at what velocity the object approaches or gets farther away from the position of the satellite. Velocity values calculated from multiple images were imported into GRASS GIS 7.2.0. and further actions were only carried out on the area of interest. Maps were generated in QGIS 2.16.14.

RESULTS

SPATIOTEMPORAL BEHAVIOUR OF SCATTERERS

During the processing phase we analysed all Sentinel-1 archive resources, which meant increased processing time as the number of images exceeded the image numbers of the former sensors manifold. All the three sensors indicate lower point densities for the area of interest than for the residential areas. In general, higher point densities were measured in descending geometries than in ascending geometries. Table 2 indicates the low point density of ERS and Envisat images compared to the results of Sentinel-1. The spatial distribution of scatterers (obtained from three different sensors) in the area of interest showed a heterogeneous pattern.

Scatterers were concentrated on the engineered structures and objects (Fig. 2) of the village. Only the Sentinel descending and Envisat ascending geometry provide scatterers for the uncovered part of the floodplain (labelled as *es* and indicated by arrows on Figures 2B and 2A). The best overlap was found

Table 2

The number of scatterers obtained during image processing for the sensors, geometries and the landslide-affected area of interest (based on own sources)

ERS				Envisat								Sentinel-1							
Descending				Ascending				Descending				Ascending				Descending			
Residential		Endangered sl.		Residential		Endangered sl.		Residential		Endangered sl.		Residential		Endangered sl.		Residential		Endangered sl.	
num.	des.	num.	des.	num.	des.	num.	des.	num.	des.	num.	des.	num.	des.	num.	des.	num.	des.	num.	des.
651	407	53	148	416	260	62	173	745	466	116	324	2525	1579	449	1254	2215	1385	660	1844

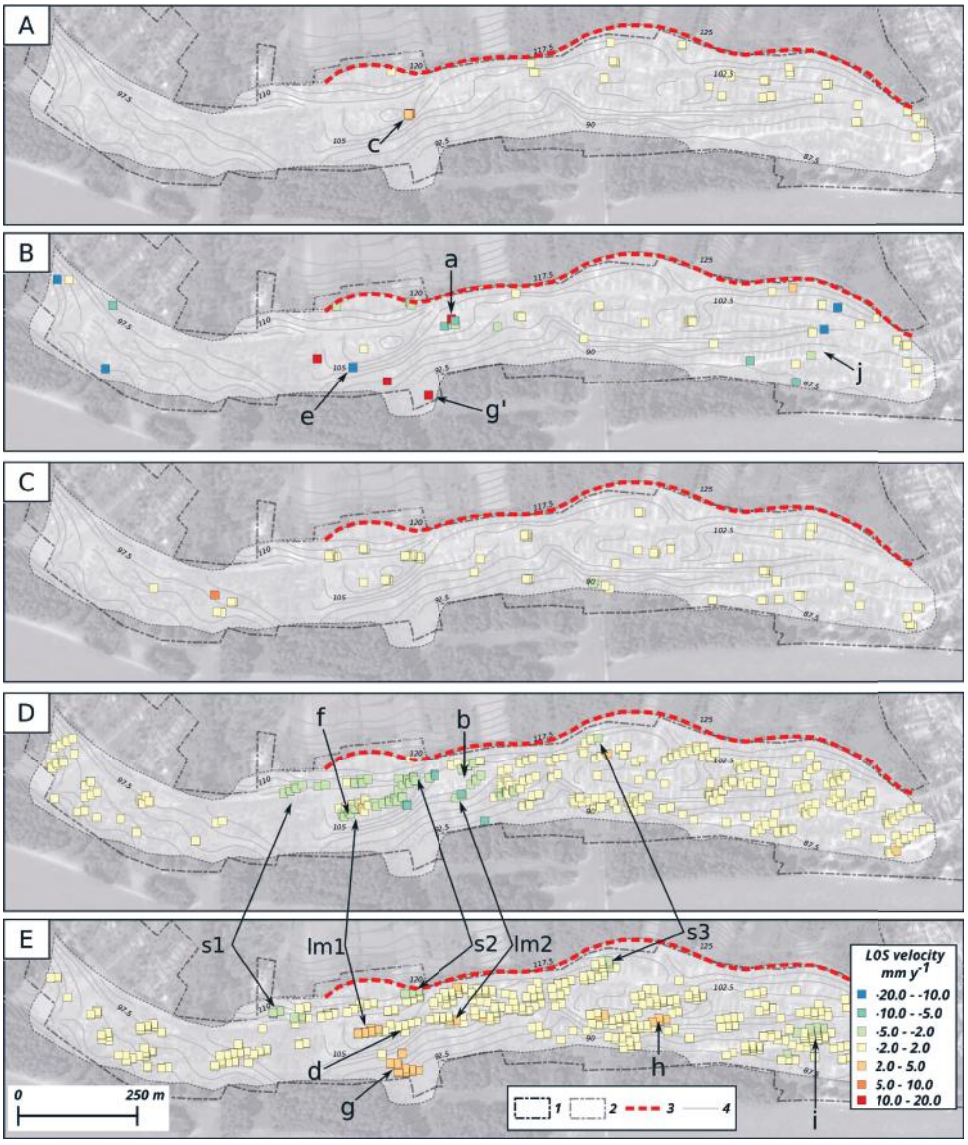

Fig. 3: LOS displacements (mm y^{-1}). A = ERS descending PSI, B = Envisat ascending PSI, C = Envisat descending PSI, D = Sentinel ascending PSI, E = Sentinel descending PSI, 1 = residential area, 2 = landslide-affected slopes, 3 = scarp (edge of high bluff), 4 = contour line (2.5 m increment), a - j = displacement zones, f = abandoned houses, lm1 – lm2 = zones of lateral movements, s1 – s3 = zones of subsidence

between Sentinel-1 geometries, however there are several dissected small areas covered only one geometry of Sentinel-1.

The displacement history of the scatterers on Figure 4 shows a marked difference among the ERS, Envisat and Sentinel-1 sensors. In the case of the Sentinel-1 data a relatively higher standard deviation of the data is found, while for

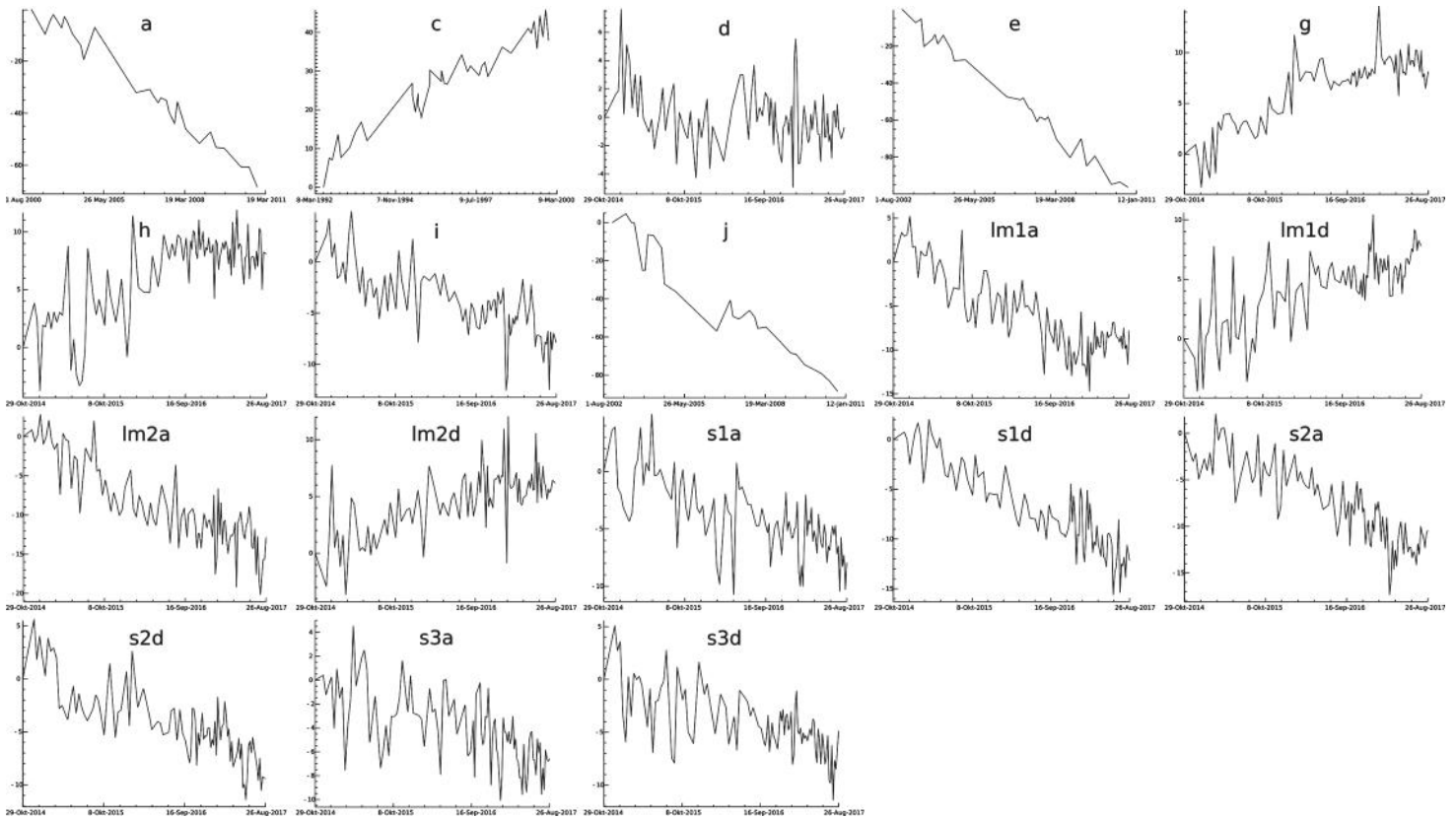

Fig. 4: LOS displacement time series (mm y^{-1}) from the Dunaszekcső study site. (Point locations are shown on Figure 2.)

the earlier sensors this value is significantly lower. The deviation of the Sentinel-1 data is around a few mm, which is likely induced by the thermal expansion of the scatterers.

DETECTED DISPLACEMENTS

Sentinel-1 ascending and descending data indicate a higher degree of overlap than in the case of the earlier sensor designs. Hence, description and interpretation of spatial blocks with different movement trends were done according to Sentinel-1 results. Velocities derived from ERS and Envisat imagery were considered additional data, which could extend time series of points and provide long term movement history of the identified blocks in case of spatial overlap with later imagery.

At the bottom of the high bluffs three groups of scatterers were identified (*s1*, *s2* and *s3* on Figures 3D and 3E) which move away from the sensors in both geometries. Area *s1* moves away from the sensor at a velocity of –2.5 mm y^{-1} in ascending geometry, while this value increase to –3.5 mm y^{-1} in descending geometry. Area *s2* moved at velocities of –3.5 to –2.5 and –2.5 mm y^{-1} in ascending and descending geometry, respectively. Area *s3*, located north of area *s2* moved at a velocity of –2.5 mm y^{-1}on the ascending orbit and at –2.0 mm y^{-1} in descending geometry. Scatterers has been moving away at a uniform velocity from the Sentinel-1 sensors. Therefore, we may assume the presence of a series smaller subsidence units (*s1, s2* and *s3* on Figure 3D and 3E). Unfortunately, no scatterers were detected here when earlier images were analysed, therefore active and ongoing movements here can only be verified here since 2014.

Further to the east from the previous zone displacements were observed on the Sentinel images (letters *b* and *f* on Figures 3D, 4b and 4lm1a), as scatterers move away from the sensor. These zones are also present on Envisat imagery, where velocities of –2 to –8 mm y^{-1} were measured (letters *a* and *e* on Figures 3B, 4a and 4e). Envisat and Sentinel-1 data indicate active mass movements of different rates here between 2002 and 2017.

Considering the surroundings of the mentioned points and both geometries of Sentinel-1, two distinct groups (*lm1*, l*m2* on Figures 3D and 3E) of scatterers can be identified, where scatterers moved toward the satellite on the ascending orbit while moved away in descending geometry (*lm1a*, *lm1d*, *lm2a* and *lm2d* on Figure 4). The *lm1* area on the ascending path moved away from the sensor at velocities of –2.5 to 3 mm y^{-1} while on the descending path it moved toward the sensor at velocities of 2 to 2.5 mm y^{-1}. The area north of *lm1* moved at velocities of –4 to –3 5 mm y^{-1} and +1.5 to 2.5 mm y^{-1} when data were derived from the ascending and descending orbits, respectively. The movement of scatterers toward the satellite on the descending path and their increasing distance (*lm1a*, *lm1d*, *lm2a* and *lm2d* on Figure 4) from the sensor in ascending geometry likely indicates their lateral (horizontal) displacement. Moreover, the rate of movement

away from the satellite in ascending geometry is higher than the rate of movement toward the sensor is descending geometry. Therefore, the actual 2-dimensional movement has two components, a weaker subsidence part and a more robust horizontal, eastward-moving element. Two abandoned houses were found and observed (location of Photos 1 and 2 is marked with letter *f* on Figure 3) at the same location, where external deformations and cracks unambiguously indicate the calculated lateral movements.

The edge of the floodplain (letter *g* on Figures 3E and 4g) and the north-central portion of the study site (letter *h* on Figures 3E and 4h), moves toward the satellite on the descending path. Scatterers indicated by letter *g* reached mean velocities of +2 to +4.9 mm y^{-1} while area *h* was moving at velocities of +1.8 – –+3.5 mm y^{-1}. Movement of part of the floodplain towards the satellite was observed in ascending geometry of the Envisat images (marked with letter *g'* on Figure 3B). This zone remains incoherent (Fig. 3C) on the images taken on descending orbit and no scatterers were identified. Location *h* remain undetected in other geometries and sensors hence any further interpretation of the deformations is questionable here.

Besides these scatterers a group of a few points moves away in a more or less uniform fashion from the satellite in the northern part of the study site (*I* on Figures 3E and 4i). Areas *I* and *j* move away from the satellite at –2.5 mm y^{-1} and –2 mm y^{-1}, respectively. Scatterers only slightly overlap the Envisat data obtained on the ascending orbit (Figs. 3B and 4j).

Photo 1. Building damage on an abandoned house at the southern part of Dunaszekcső. Foundation of the house was broken.

Photo 2. Damages to a residential property at the southern part of Dunaszekcső. Foundation and the walls of the house were ruptured due to shear stresses.

Point *d* (Figs. 3E and 4d) indicates stable surface in descending geometry of Sentinel-1 and non-coherent in the ascending geometry. Point *d* overlaps point *c* (Fig. 3A) derived from ERS imagery and the point moved towards the sensor. The mean velocity of this point was +4.7 mm y^{-1}. This point appeared as a non-coherent surface on the subsequent Envisat images (Fig. 3B), hence no information is available on its movement history for the period of 2002 to 2010.

Other scatterers with velocities higher than 15 mm y^{-1} and lower than –15 mm y^{-1} are also observed on the Envisat ascending images (Fig. 3B) but Sentinel or ERS imagery. Scatterers with velocities of less than –15 mm y^{-1} are located on the southern and northern part of the study area. Nonetheless, due to their sporadic distribution, they do not indicate a distinct spatial pattern.

DISCUSSION

The Sentinel-1 interferometric results significantly exceed the coverage/scatterer density obtained by the earlier sensors (Del Ventisette et al. 2013). The differences in the number of scatterers in ascending and descending geometries follow from the topography of the test site (Ferretti 2014).

The difference of spatial densities of the Sentinel-1 and older sensors is interpreted in the light of the lower (25 m) resolution of ERS and Envisat sensors and the advanced (15 m) pixel size of Sentinel-1. In addition, the new acquisition technique (TOPSAR) of Sentinel-1 (shorter Bts and advanced temporal image

separation) preserves the coherence, hence increased number of scatterers are found. However, the low spatial coverage of ERS and Envisat scatterers is not only caused by their lower spatial resolution but by the poor temporal separation of the images. The loss of coherence may also be the consequence of both the ERS and Envisat time series when movement velocity exceeds the detectable range of the sensor (½ λ/Bt). When high velocities are detected by the sensors the temporal coherence may be interrupted and are not found. Hence the surface segments with high velocities will not be present as scatterers on the final velocity image. It may be the reason why low scatterer density is present on the area of interest compared to other parts of the village. However, another explanation can be the sparse spatial appearance of engineered structures and objects in the area of interest.

Owing to the better temporal separation of the data, the impact of the deviation of thermal expansion is more pronounced in the Sentinel images compared to the earlier sensors, because Sentinel imagery offer fine temporal resolution. Therefore, to better understand the deformation- and landslide-triggered displacement behaviour, thermal properties and expansion characteristics of the media (sediments) should be analysed, and, if necessary, thermal noise should be filtered.

According to our findings the landslide-affected slopes do not move as one large block but rather as multiple small units. It has already been reported that individual landslide blocks along the Danube's high bluff move independently from their surroundings (Újvári et al. 2009; Kovács et al. 2015) most typically on the vertical wall in the village of Dunaszekcső. C. Del Ventisette et al. (2013) investigated the Rácalmás Landslide, which has a geomorphological setting similar to the study site presented in the current paper. The authors also categorized surface segments of active landslides of similar displacement velocities based on ERS and Envisat data. However, 2D movements have not been observed there. Additionally, according to our observations based on Sentinel-1 imagery the Rácalmás Landslide shows the same spatial trends as the Dunaszekcső test site (paper under revision in the journal Natural Hazards).

The interpretation of displacements is highly encumbered due to the non-perfect overlap between Sentinel-1 geometries and older sensors in the recent test site. Hence, both the spatial and the temporal data show a mosaic pattern in the area of interest. Distinct subsidence at the bottom of the main scarp, lateral movements of the middle part of the area and uplift and the lateral movement of the floodplain indicate slow creeping or sliding of former landslide materials. However, displacements are not uniform spatially and temporally. The lateral displacement towards the Danube in the middle of the area of interest are distinct and clearly observable. This finding is validated by the rupture and displacement structure on two buildings (Photos 1 and 2). However, validation of slow displacement in the range of a few mm y^{-1} is doubtful as other houses in the village have been maintained at a regular basis. Both abandoned houses,

however, are located in an active landslide zone, where mass movements have been confirmed for the past 25 years, therefore their impacts are more obvious.

Displacements on the floodplain of the Danube were detected by Envisat and Sentinel-1 sensors. However, movement toward the sensor in Envisat ascending geometry can be interpreted in two ways. Firstly, it may refer the uplift of the area or may indicate the horizontal, westward movement of the floodplain. The latter theory may be ignored due to the geomorphologic position of the area, as the landslide blocks or their immediate foreground is unable to move uphill since gravitational potential points to the low-lying floodplain in the immediate foreground. Also, there is no such a mass in the foreground which could trigger the block rotation or upthrusting of the compressed foot of the landslide. The movement toward the sensors in Sentinel descending geometry is interpreted as vertical uplift and is explained by several factors. The scatterers are positioned on the margin of the Danube channel, where large amounts of silt have been deposited, and sediment accumulation is reflected as increasing surface elevation on the images. Additionally, the deformation of the *im1* zone, located above the bank may also trigger vertical displacements. According to the latter, the movement of the scatterers to the Sentinel-1 sensor in descending geometry is interpreted as an eastward oriented dislocation. Smaller displacement zones are also observed in the area (*h* and *i* on Figure 3E and *j* on Figure 3B). The dislocation of zone *h* is only verified by data from the Sentinel-1 descending geometry (*h* on Figure 4), however, the data becomes incoherent in other images obtained with other satellites and geometry. Similarly, zone *i* (*I* on Figure 4) also moved away from the sensor according to Envisat ascending orbit data. The two temporally distant data implies the continuous subsidence of the area, however, at least two uncertainties are associated with this statement: (i) absence of scatterers in Envisat descending orbit and (ii) the time elapse of four years between the Envisat and Sentinel-1 stacks).

CONCLUSIONS

Scatterer density of interferometric data, derived from Sentinel-1 images, far exceeds the spatial coverage obtained by the earlier sensors. The two orbital geometries (ascending and descending) enable larger spatial coverage and due to the overlap between the two orbital datasets, permit the detection of horizontal 2D displacements. However, the comparison of the two geometries is only possible for small areas. The studied area indicated partial stability between 1992 and 2010 by Envisat and ERS data, yet some areas may be in motion, but movement rates are beyond or below the detection range of the sensors. Some of the displacements of this period may be tracked on Sentinel data, and their displacement history for the past 25 years may be interpreted. The displacement data in the central part of the study site indicate the subsidence of the sliding

block along the escarpment, while to the east it is moving towards the Danube. This displacement then triggers the uplift of the floodplain edges, or generates a slight eastward displacement. These movements seem to be similar to the surface displacements at the northern high buff of the Danube at Rácalmás.

Apart from the previously discussed example, displacement history and spatial distribution of displacements are heterogeneous in the study site. Field validation of the measurements and exploration of surface deformation in areas devoid of scatterers makes further research indispensable for the better understanding of deformation behaviours and patterns of the high bluff sections along the Hungarian reaches of the Danube.

Moreover, to increase prediction accuracy, locate deformations and to better understand the influence of climate and water level changes on mass movements, temporal behaviour of landsides should be correlated with available climate and water regime data.

ACKNOWLEDGEMENT

The corresponding author is grateful to P. Pasquali and F. Holecz for the personal research grant and to Sarmap SA staffs for their kind contribution on SAR image processing. The authors are grateful to the Doctoral School of Earth Sciences at the University of Pécs and its director, Professor Z. Dövényi for funding the current project.

The present scientific contribution is dedicated to the 650th anniversary of the foundation of the University of Pécs, Hungary.

[1] *University of Pécs, Faculty of Sciences, Institute of Geography and Earth Sciences, Dept. of Cartography and GIS, 7624 Pécs Ifjúság Str. 6., Hungary*

[2] *University of Pécs, Faculty of Sciences, Institute of Geography and Earth Sciences, Dept. of Physical and Environmental Geography, 7624 Pécs Ifjúság Str. 6, Hungary*

[3] *Sarmap SA, Cascio di Barico 10, Purasca, Switzerland*

** e-mail of the corresponding author: vonbock@gamma.ttk.pte.hu*

REFERENCES

Balogh J., Schweitzer F., 2011. *Felszínmozgásos folyamatok a Duna Gönyű–Mohács közötti magasparti szakaszain (Mass movements along the Danubian high bluff between Gönyű and Mohács).* [in:] F. Schweitzer (ed.), *Katasztrófák tanulságai. Stratégiai jellegű természetföldrajzi kutatások* (*Conclusions of catastrophes. Physical geographical researches for strategic purposes)*. Magyar Tudományos Akadémia Földrajztudományi Kutatóintézete, Budapest, 101–142.

Bányai L., Mentes Gy., Újvári G., Kovács M., Czap Z., Gribovszki K., Papp G., 2014. *Recurrent landsliding of a high bank at Dunaszekcső, Hungary: Geodetic deformation monitoring and finite element modelling.* Journal of Geodynamics 47, 130–141.

Bugya T., Fábián Sz.Á., Görcs N. L., Kovács I.P., Radvánszky B, 2011. *Surface changes on a landslide affected high bluff in Dunaszekcső (Hungary)*. Central European Journal of Geosciences 3, 119–128.

Chen Q., Cheng H., Yang Y., Liu G., Liu L., 2014. *Quantification of mass wasting volume associated with the giant landslide Daguangbao induced by the 2008 Wenchuan earthquake from persistent scatterer InSAR*. Remote Sens. Environ. 152, 125–135.

Del Ventisette C., Ciampalini A., Calò F., Manunta M., Paglia L., Reichenbach P., Colombo D., Mora O., Strozzi T., Garcia I., Mateos R., Herrera G., Füsi B., Graniczny M., Przylucka M., Retzo H., Moretti S., Casagli N., Guzzetti F., 2013. *Exploitation of large archives of ERS and ENVISAT C-Band SAR data to characterize ground deformation.* Remote Sensing 5, 3896–3917.

Dövényi Z., 2010. Magyarország *kistájainak katasztere (Inventory of microregions in Hungary).* MTA Földrajztudományi Kutatóintézet, Budapest.

Egri Gy., Párdányi J., 1968. *Dunaújvárosi magaspartok állékonyság vizsgálata (Sability analysis of high bluffs at Dunaújváros)*. Műszaki Tervezés (Engineering Design) 7, 19–24.

ESA 2013 Sentinel-1 User Handbook, Online 29.12.2017 https://sentinels.copernicus.eu/documents/247904/685163/Sentinel-1_User_Handbook.

Ferretti A., Prati C., Rocca F., 2001. *Permanent scatterers in SAR interferometry.* IEEE Transactions on Geoscience and Remote Sensing 39, 8–20.

Ferretti A., 2014. *Satellite InSAR data. Reservoir monitoring from space*. EAGE Publications, The Netherlands.

Ferretti A., Prati C., Rocca F., 2000. *Nonlinear subsidence rate estimation using permanent scatterers in differential SAR interferometry*. IEEE Transactions on Geoscience and Remote Sensing 38, 2202–2212.

Fodorné T., Horváth Zs., Scheuer Gy., Schweitzer F., 1981. *Dunakömlőd–Paks közötti dunai magaspart mérnökgeológiai térképezése és vizsgálata (Engineering geological mapping of the high bluff between Dunakömlőd and Paks)*. Földtani Közlöny (Bulletin of the Hungarian Geological Society) 111, 258–280.

Glade T., Anderson M., Crozier M.J., (eds.) 2005. *Landslide Hazard and Risk*. John Wiley and Sons, Chichester.

Györké Z., Scheuer Gy., Vágóné I., 1975. *Magaspartok állékonyságvizsgálata (Analysis of the stability of high bluffs).* FTI Évkönyv (FTI year-book) 1950–1975, 133–138.

Hein A., 2004. *Processing of SAR data, Fundamentals, signal processing, interferometry.* Springer, Berlin, Heidelberg New York.

Herrera G., Gutiérrez F., García-Davalillo J.C., Guerrero J., Notti D., Galve J.P., Fernández-Merodo J.A., Cooksley G., 2013. *Multi-sensor advanced DInSAR monitoring of very slow landslides: the Tena Valley case study (Central Spanish Pyrenees)*. Remote Sens. Environ. 128, 31–43.

Herrera G., Notti D., García-Davalillo J.C., Mora O., Cooksley G., Sánchez M., Arnaud A., Crosetto M., 2010. *Analysis with C- and X-band satellite SAR data of the Portalet landslide area.* Landslides 8, 195–206.

Horváth Zs., Scheuer Gy., 1976. *A dunaföldvári partrogyás mérnökgeológiai vizsgálata (Engineering geological analysis of surface displacements at Dunaföldvár).* Földtani Közlöny (Bulletin of the Hungarian Geological Society) 106, 425–440.

Horváth Zs., Szilvágyi I., Szörényi J., 1975. *Csúszásveszélyes területek vizsgálata és nyilvántartása (The analysis and inventory of areas hazarded by landslides)*. FTI Évkönyv (FTI yearbook) 1950–1975, 130–132.

Karácsonyi S., Scheuer Gy., 1972. *A dunai magaspartok építésföldtani problémái (Engineering geological problems of the Danubian high bluffs)*. Földtani Kutatás (Geological Research) 15, 71–83.

Kaszás F., Kraft J., 2009. *A dunaszekcsői magaspart rogyásos suvadása: Nem nyugszanak a dunai magaspartok! (Landslides of the Dunaszekcső high bluff: High bluffs are active!)*. Mélyépítő tükörkép magazin (Civil Engineering Magazine) 8, 35–39.

Kenesei J., Marokházi G., Nagy J., 2005. *Mozgásveszélyes Duna-menti és Balaton parti magaspartok veszélyelhárítási munkáinak tanulmányterve (Plan of the prevention works at landslide endangered high bluffs along the Danube and the Lake Balaton)*. Manuscript.

Kézdi Á., 1970. *A dunaújvárosi partrogyás (Landslide at Dunaújváros).* Mélyépítéstudományi Szemle (Civil Engineering Review) 20, 281–297.

Kovács I. P., Fábián Sz. Á., Radvánszky B., Varga G., 2015. *Dunaszekcső Castle Hill: Landslides Along the Danubian Loess Bluff*. [in:] D. Lóczy (ed.), *Landscapes and Landforms of Hungary*. Springer International, Switzerland, 113–120.

Kraft J., 2011. *Dunai magaspart dunaszekcsői részletének rogyásos suvadásai (Landslides of the Dunaszekcső high bluff).* [in:] Á. Török, B. Vásárhelyi (eds.), *Mérnökgeológia – Kőzetmechanika (Engineering geology – Rock mechanics)*. Hantken Kiadó, Budapest, 93–104.

Moyzes A., Scheuer Gy., 1978. *A dunaszekcsői magaspartok mérnökgeológiai vizsgálata (Engineering geological analysis of the Dunaszekcső high bluff)*. Földtani Közlöny (Bulletin of the Hungarian Geological Society) 108, 213–226.

Pasquali P., Cantone A., Riccardi P., Defilippi M., Ogushi F., Gagliano S., Tamura M., 2014. *Mapping of ground deformations with interferometric stacking techniques.* [in:] F. Holecz, P. Pasquali, N. Milisavljevic (eds.), *Land applications of radar remote sensing*. Intech, DOI: 10.5772/55833, 234–259.

Pécsi M., 1956. *Adatok a fiatal kéregmozgások szerepére és mértékére a Duna völgyben (Data on the role and rate of crustal movements in the Danube Valley).* Tud. Gyűjtemény (Scientific Collection) 9, 13–26.

Pécsi M., 1959. *A magyarországi Dunavölgy kialakulása és felszínalaktana (The geomorphology and surface development of the Danube Valley).* Akadémiai Kiadó, Budapest.

Pécsi M., 1971. *Az 1970. évi Dunaföldvári földcsuszamlás*. Földrajzi Értesítő (Hungarian Geographical Bulletin) 19, 233–238.

Pécsi M., Schweitzer F., 1995. *The lithostratigraphical, chronostratigraphical sequence of Hungarian loess profiles and their geomorphological position.* Loess in Form 3, 31–61.

Scheuer Gy., 1979. *A dunai magaspartok mérnökgeológiai vizsgálata (Engineerig geological analysis of Danubian high bluf).* Földtani Közlöny (Bulletin of the Hungarian Geological Society) 109, 230–254.

Schmiedt E.R., 1966. *A dunaújvárosi 1964. évi partomlás (Bank failure at Dunaújváros in 1964).* MÁFI Évi Jelentése 1964 (Annual Report of the Hungarian Geological Society on 1964), 579–584.

Singleton A., Li Z., Hoey T., Muller J.P., 2014. *Evaluating sub-pixel offset techniques as an alternative to D-InSAR for monitoring episodic landslide movements in vegetated terrain*. Remote Sens. Environ. 147, 133–144.

Sowter A., Bin Che Amat M., Cigna F., Marsh S., Athab A., Alshammari L., 2016. *Mexico City land subsidence in 2014–2015 with Sentinel-1 IW TOPS: Results using Intermittent SBAS (ISBAS) technique*. International Journal of Applied Earth Observation and Geoinformation 52, 230–242.

Tomás R., Li Z., Liu P., Singleton A., Hoey T., Cheng X., 2014. *Spatiotemporal characteristics of the Huangtupo landslide in the Three Gorges region (China) constrained by radar interferometry.* Geophys. J. Int. 197, 213–232.

Tóth I., Scheuer Gy., Vermes J., 1968. *Mérnökgeológiai megfigyelések a rácalmási suvadással kapcsolatban (Engineering geological observations at the Rácalmás landslide).* Mérnökgeológiai Szemle (Engineering Geology Review) 4, 13–27.

Újvári G., Mentes Gy., Bányai L., Kraft J., Gyimóthy A., Kovács J., 2009. *Evolution of a bank failure along the River Danube at Dunaszekcső, Hungary.* Geomorphology 109, 197–209.

Wasowski J., Bovenga F., 2015. *Remote sensing of landslide motion with emphasis on satellite multitemporal interferometry applications: an overview*. [in:] T. Davies (ed.*), Landslide hazards, risk, and disasters*. Elsevier, Amsterdam, 345–403.